PERGAMON

International Journal of Heat and Mass Transfer 45 (2002) 2465–2483

International Journal of HEAT and MASS TRANSFER

www.elsevier.com/locate/ijhmt

Hydromagnetic double-diffusive convection in a rectangular enclosure with opposing temperature and concentration gradients

Ali J. Chamkha *, Hameed Al-Naser

Department of Mechanical Engineering, Kuwait University, P.O. Box 5969, 13060 Safat, Kuwait

Received 8 February 2000; received in revised form 7 November 2001

Abstract

The finite-difference method is used to predict numerically the characteristics of hydromagnetic double-diffusive convective flow of a binary gas mixture in a rectangular enclosure with the upper and lower walls being insulated. Constant temperatures and concentrations are imposed along the left and right walls of the enclosure and a uniform magnetic field is applied in the x-direction. Consistent with what is reported by previous investigators, an oscillation in the flow is observed in the absence of the magnetic field for a specific range of buoyancy ratio values where the Prandtl number $Pr = 1$, the Lewis number $Le = 2$, the thermal Rayleigh number $Ra_T = 10^5$, and the aspect ratio $A = 2$ for the enclosure. In the presence of the magnetic field, however, no oscillatory behavior is observed. Numerical results are reported for the effect of the heat generation or absorption coefficient and the Hartmann number on the contours of streamline, temperature, concentration and density. In addition, results for the average Nusselt and Sherwood numbers are presented and discussed for various parametric conditions. In this study, the thermal and compositional buoyancy forces are assumed to be opposite. © 2002 Published by Elsevier Science Ltd.

1. Introduction

Natural convection is of great importance in many industrial applications. Convection plays a dominant role in crystal growth in which it affects the fluid-phase composition and temperature at the phase interface that results in a single crystal since poor crystal quality is due to turbulence. It is the foundation in modern electronics industry to produce pure and perfect crystals to make transistors, lasers rods, microwave devices, infrared detectors, memory devices, and integrated circuits. Natural convection adversely affects local growth conditions and enhances the overall transport rate. The combination of temperature and concentration gradients in the fluid will lead to buoyancy-driven flows. This has an important influence on the solidification process in a binary system. When heat and mass transfer occurs simultaneously, it leads to a complex fluid motion called double-diffusive convection. Double-diffusion occurs in a wide range of scientific fields such as oceanography, astrophysics, geology, biology and chemical processes (see, for instance, [4]). Ostrach [20] and Viskanta et al. [27] reported complete reviews on the subject. Bejan [5] reported a fundamental study of scale analysis relative to heat and mass transfer within cavities submitted to horizontal combined and pure temperature and concentration gradients. Kamotani et al. [12] considered an experimental study of natural convection in shallow enclosures with horizontal temperature and concentration gradients. Other experimental studies dealing with thermosolutal convection in rectangular enclosures were reported by Ostrach et al. [19] and Lee et al. [13]. Lee and Hyun [14] and Hyun and Lee [10] reported numerical solutions for unsteady double-diffusive convection in a rectangular enclosure with aiding and opposing temperature and concentration gradients that were in good agreement with reported experimental results. Other related numerical studies dealing with

* Corresponding author. Tel.: +965-571-2298; fax: +965-484-7131.

E-mail address: chamkha@kuc01.kuniv.edu (A.J. Chamkha).

0017-9310/02/$ - see front matter © 2002 Published by Elsevier Science Ltd.
PII: S0017-9310(01)00344-1

Nomenclature

A	enclosure aspect ratio $= H/W$
B_0	magnetic induction
c	concentration of species
c_h	high species concentration (source)
c_ℓ	low species concentration (sink)
C	dimensionless species concentration $= (c - c_\ell)/(c_h - c_\ell) - 0.5$
D	species diffusivity
g	gravitational acceleration
H	enclosure height
Ha	Hartmann number $= B_0 W\sqrt{\sigma/\mu}$
Le	Lewis number $= \alpha/D$
N	buoyancy ratio $= \beta_c(c_h - c_\ell)/[\beta_T(T_h - T_c)]$
$\overline{Nu}$	average Nusselt number
p	fluid pressure
Pr	Prandtl number $= \nu/\alpha$
Q_0	dimensional heat generation or absorption coefficient
Ra_T	thermal Rayleigh number $= g\beta_T(T_h - T_c)W^3/(\alpha\nu)$
$\overline{Sh}$	average Sherwood number
t	time
t_0	period of oscillation
T	temperature
T_h	hot wall temperature (source)
T_c	cold wall temperature (sink)
u	horizontal velocity component
U	dimensionless horizontal velocity component $= uW/\alpha$
v	vertical velocity component
V	dimensionless vertical velocity component $= vW/\alpha$
W	enclosure width
x	horizontal coordinate
X	dimensionless horizontal coordinate $= x/W$
y	vertical coordinate
Y	dimensionless vertical coordinate $= y/W$

Greek symbols

α	thermal diffusivity
β_T	thermal expansion coefficient
β_c	compositional expansion coefficient
ϕ	dimensionless heat generation or absorption $= Q_0 W^2/(\rho c_p \alpha)$
μ	dynamic viscosity
ν	kinematic viscosity $= \mu/\rho$
θ	dimensionless temperature $= (T - T_c)/(T_h - T_c) - 0.5$
ρ	density
ρ^*	dimensionless density $= NC - \theta$
σ	electrical conductivity
τ	dimensionless time $= \alpha t/W^2$
τ_0	dimensionless period of oscillation $= \alpha t_0/W^2$
Ω	vorticity
Ψ	dimensionless stream function $= \Psi/\alpha$
ψ	stream function
ζ	dimensionless vorticity $= \Omega W^2/\alpha$
∇^2	Laplacian operator

double-diffusive natural convection in cavities were considered by Ranganathan and Viskanta [22], Trevisan and Bejan [25], Beghein et al. [4] and Nishimura et al. [17].

Electrically conducting fluids in the presence of a magnetic field have been used extensively in many applications such as crystal growth. Oreper and Szekely [18] have found that the presence of a magnetic field can suppress natural convection currents and that the strength of the magnetic field is one of the important factors in determining the quality of the crystal. Ozoe and Maruo [21] have investigated magnetic and gravitational natural convection of melted silicon-two dimensional numerical computations for the rate of heat transfer. Garandet et al. [9] and Alchaar et al. [2] have considered natural convection heat transfer in a rectangular enclosure with a transverse magnetic field. Rudraiah et al. [23] and Al-Najem et al. [3] have studied the effects of a magnetic field on free convection in a rectangular enclosure.

Natural convection heat transfer induced by internal heat generation has recently received considerable attention because of numerous applications in geophysics and energy-related engineering problems. Such applications include heat removal from nuclear fuel debris, underground disposal of radioactive waste materials, storage of foodstuff, and exothermic chemical reactions in packed-bed reactor (see, for instance, [11]). Acharya and Goldstein [1] studied numerically two-dimensional natural convection of air in an externally heated vertical or inclined square box containing uniformly distributed internal energy sources. Their numerical results showed two distinct flow pattern systems depending on the ratio of the internal to the external Rayleigh numbers. Also, it was found that the average heat flux ratio along the cold wall increased with increasing external Rayleigh numbers and decreasing internal Rayleigh numbers. Recently, Churbanov et al. [8] studied numerically unsteady natural convection of a heat generating fluid in a vertical rectangular enclosure with isothermal or adiabatic rigid walls. Their results were obtained using a finite-difference scheme in the two-dimensional stream function-vorticity formulation.

Steady-state as well as oscillating solutions were obtained and compared with other numerical and experimental published data. Other related works dealing with temperature-dependent heat generation effects can be found in the papers by Vajravelu and Nayfeh [26] and Chamkha [7].

In this paper, the problem of unsteady, laminar, hydromagnetic, double-diffusive natural convection flow inside a rectangular enclosure in the presence of heat generation or absorption is considered.

2. Mathematical model

The schematic of the system under consideration is shown in Fig. 1. The temperatures T_h and T_c are uniformly imposed along the left and right walls and the top and bottom walls are assumed to be adiabatic and impermeable to mass transfer. The left wall is the source where the mixture diffuses to the right wall (sink). A magnetic field with uniform strength B_0 is applied in the x-direction. Also, the enclosure is filled with a binary mixture of gas. The fluid is assumed to be incompressible, Newtonian, electrically conducting, heat generating or absorbing and viscous. The viscous dissipation and magnetic dissipation are all assumed to be negligible. The magnetic Reynolds number is assumed to be so small that the induced magnetic field is neglected. The Boussinesq approximation with opposite thermal and compositional buoyancy forces is used for the body force terms in the momentum equations.

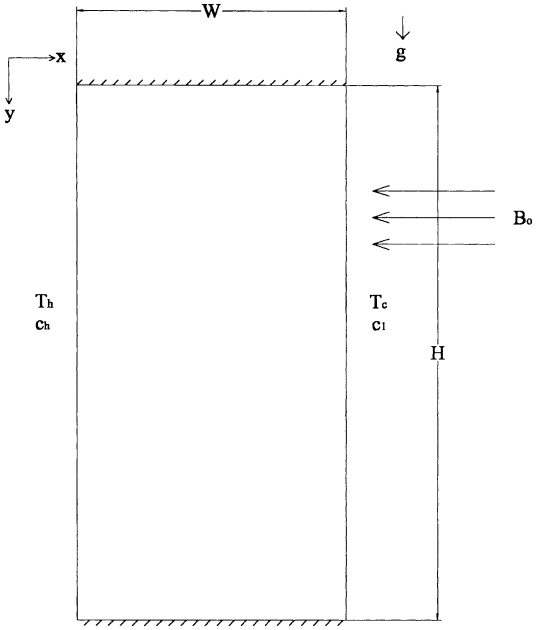

Fig. 1. Schematic diagram and coordinate system.

The governing equations for the problem under consideration are based on the balance laws of mass, linear momentum, thermal energy and concentration in two dimensions. Following the previous assumptions, these equations can be written in dimensional form as

$$\frac{\partial u}{\partial x}+\frac{\partial v}{\partial y}=0, \tag{1}$$

$$\frac{\partial u}{\partial t}+u\frac{\partial u}{\partial x}+v\frac{\partial u}{\partial y}=-\frac{1}{\rho}\frac{\partial p}{\partial x}+v\left(\frac{\partial^2 u}{\partial x^2}+\frac{\partial^2 u}{\partial y^2}\right), \tag{2}$$

$$\frac{\partial v}{\partial t}+u\frac{\partial v}{\partial x}+v\frac{\partial v}{\partial y}=-\frac{1}{\rho}\frac{\partial p}{\partial y}+v\left(\frac{\partial^2 v}{\partial x^2}+\frac{\partial^2 v}{\partial y^2}\right) -g\beta_T(T-T_c)+g\beta_c(c-c_\ell)-\frac{\sigma B_0^2}{\rho}v, \tag{3}$$

$$\frac{\partial T}{\partial t}+u\frac{\partial T}{\partial x}+v\frac{\partial T}{\partial y}=\alpha\left(\frac{\partial^2 T}{\partial x^2}+\frac{\partial^2 T}{\partial y^2}\right)+\frac{Q_0}{\rho c_p}(T-T_c), \tag{4}$$

$$\frac{\partial c}{\partial t}+u\frac{\partial c}{\partial x}+v\frac{\partial c}{\partial y}=D\left(\frac{\partial^2 c}{\partial x^2}+\frac{\partial^2 c}{\partial y^2}\right), \tag{5}$$

where u and v are the velocity components in the x- and y-directions. β_T and β_c are the thermal and compositional expansion coefficients, respectively. x, y and t are the horizontal and vertical distances and time, respectively. p, T and c are the pressure, temperature and concentration, respectively. α, v, c_p, and ρ are the fluid thermal diffusivity, kinematic viscosity, specific heat at constant pressure and fluid density, respectively. D is the species diffusivity, T_h and T_c are the hot and cold wall temperatures, c_h and c_ℓ are the concentrations at the hot and cold walls, and g is the gravitational acceleration. σ, B_0, Q_0 are the electrical conductivity, magnetic induction, and the dimensional heat generation or absorption coefficient, respectively.

The initial and boundary conditions for the problem can be written as

$$\begin{aligned}
&t=0: \quad u=0,\ v=0,\ T=T_c,\ c=c_\ell,\\
&x=0,\ y=y: \quad u=0,\ v=0,\ T=T_h,\ c=c_h,\\
&x=W,\ y=y: \quad u=0,\ v=0,\ T=T_c,\ c=c_\ell,\\
&x=x,\ y=0: \quad u=0,\ v=0,\ \frac{\partial T}{\partial y}=0,\ \frac{\partial c}{\partial y}=0,\\
&x=x,\ y=H: \quad u=0,\ v=0,\ \frac{\partial T}{\partial y}=0,\ \frac{\partial c}{\partial y}=0,
\end{aligned} \tag{6}$$

where W and H are the width and height of the enclosure, respectively.

The stream function and vorticity can be defined in the usual way as

$$u=\frac{\partial \Psi}{\partial y}, \quad v=-\frac{\partial \Psi}{\partial x}, \quad \Omega=-\left(\frac{\partial^2 \Psi}{\partial x^2}+\frac{\partial^2 \Psi}{\partial y^2}\right), \tag{7}$$

where Ψ is the dimensional stream function and Ω is the dimensional vorticity.

Eqs. (1)–(7) are nondimensionalized using the following dimensionless variables:

$$\zeta = \frac{\Omega W^2}{\alpha}, \quad \psi = \frac{\Psi}{\alpha}, \quad \theta = \frac{(T - T_c)}{(T_h - T_c)} - 0.5,$$
$$C = \frac{(c - c_\ell)}{(c_h - c_\ell)} - 0.5, \quad X = \frac{x}{W}, \quad Y = \frac{y}{W},$$
$$\tau = \frac{\alpha t}{W^2}, \quad Pr = \nu/\alpha, \quad Ha = B_0 W \sqrt{\frac{\sigma}{\mu}}, \tag{8}$$
$$N = \frac{\beta_c (c_h - c_\ell)}{\beta_T (T_h - T_c)}, \quad Le = \frac{\alpha}{D},$$
$$Ra_T = \frac{g\beta_T (T_h - T_c) W^3}{\alpha \nu}, \quad \phi = \frac{Q_0 W^2}{\rho c_p \alpha}.$$

The dimensionless parameters appearing in the above equations are the Prandtl number (Pr), the Lewis number (Le), the thermal Rayleigh number (Ra_T), the Hartmann number (Ha), the dimensionless heat generation or absorption coefficient (ϕ) and the buoyancy ratio (N). ζ is the dimensionless vorticity, and ψ is the dimensionless stream function. τ is the dimensionless time. X and Y are the dimensionless x- and y-coordinates. θ and C are the dimensionless temperature and concentration.

By employing Eq. (8), the resulting dimensionless equations (after eliminating the pressure gradient terms) can be written as

$$\zeta = \frac{\partial V}{\partial X} - \frac{\partial U}{\partial Y} = -\nabla^2 \psi, \tag{9}$$

$$\frac{\partial \zeta}{\partial \tau} + U\frac{\partial \zeta}{\partial X} + V\frac{\partial \zeta}{\partial Y} = Pr\nabla^2 \zeta + Ra_T Pr\left(-\frac{\partial \theta}{\partial X} + N\frac{\partial C}{\partial X}\right) - Ha^2 Pr\frac{\partial V}{\partial X}, \tag{10}$$

$$\frac{\partial \theta}{\partial \tau} + U\frac{\partial \theta}{\partial X} + V\frac{\partial \theta}{\partial Y} = \nabla^2 \theta + \phi[\theta + 0.5], \tag{11}$$

$$\frac{\partial C}{\partial \tau} + U\frac{\partial C}{\partial X} + V\frac{\partial C}{\partial Y} = \nabla^2 C/Le. \tag{12}$$

The dimensionless initial and boundary conditions become

$\tau = 0$:

$$U = V = \psi = 0, \quad \theta = -0.5, \quad C = -0.5, \tag{13a}$$

$Y = 0$ (*horizontal top wall*):

$$U = V = \psi = 0, \quad \zeta = -\left(\frac{\partial^2 \psi}{\partial Y^2}\right), \quad \frac{\partial \theta}{\partial Y} = 0, \quad \frac{\partial C}{\partial Y} = 0, \tag{13b}$$

$Y = H/W$ (*horizontal bottom wall*):

$$U = V = \psi = 0, \quad \zeta = -\left(\frac{\partial^2 \psi}{\partial Y^2}\right), \quad \frac{\partial \theta}{\partial Y} = 0, \quad \frac{\partial C}{\partial Y} = 0, \tag{13c}$$

$X = 0$ (*vertical left wall*):

$$U = V = \psi = 0, \quad \zeta = -\left(\frac{\partial^2 \psi}{\partial X^2}\right), \quad \theta = 0.5, \quad C = 0.5, \tag{13d}$$

$X = 1$ (*vertical right wall*):

$$U = V = \psi = 0, \quad \zeta = -\left(\frac{\partial^2 \psi}{\partial X^2}\right), \quad \theta = -0.5, \quad C = -0.5. \tag{13e}$$

Computations were performed numerically to solve Eqs. (9)–(13e) using a 300 MHz PC with the Fortran language. The finite-difference approximation from the Taylor series is used to solve the partial differential dimensionless equations with an aspect ratio of 2 for the rectangular enclosure. In all the results obtained $Pr = 1.0$, $Le = 2.0$ and $Ra_T = 10^5$ were used. A computational domain consisting of 31×41 grid points was used. The details for the numerical algorithm are given below.

3. Numerical algorithm

The numerical algorithm used to solve Eqs. (9)–(13e) is based on the finite-difference methodology. First, the central difference is used to approximate the second derivatives and then it is transformed to the implicit line tridiagonal equations and solved in the x-direction for the concentration, temperature, vorticity and the stream function. This method was stable and gave results that are very close to the numerical results obtained by Nishimura et al. [17] using the finite-element method.

The finite-difference formulation of Eq. (9) is

$$\zeta = -\frac{[\psi_{i+1,j}^{n+1} - 2\psi_{i,j}^{n+1} + \psi_{i-1,j}^{n+1}]}{\Delta X^2} - \frac{[\psi_{i,j+1}^{n} - 2\psi_{i,j}^{n+1} + \psi_{i,j-1}^{n}]}{\Delta Y^2}, \tag{14a}$$

which can be rearranged as

$$\psi_{i-1,j}^{n+1}[E_1] + \psi_{i,j}^{n+1}[B_1] + \psi_{i+1,j}^{n+1}[A_1] = [D_1], \tag{14b}$$

where

$$E_1 = [\Delta Y^2], \quad B_1 = [-2\Delta Y^2 - 2\Delta X^2], \quad A_1 = [\Delta Y^2],$$
$$D_1 = -\zeta_{i,j}\Delta X^2 \Delta Y^2 - \Delta X^2[\psi_{i,j+1}^{n} + \psi_{i,j-1}^{n}]. \tag{14c}$$

The finite-difference formulation for Eq. (10) will have the form

$$\frac{[\zeta_{i,j}^{n+1}-\zeta_{i,j}^{n}]}{\Delta\tau}+U_{i,j}\frac{[\zeta_{i+1,j}^{n+1}-\zeta_{i-1,j}^{n+1}]}{2\Delta X}+V_{i,j}\frac{[\zeta_{i,j+1}^{n}-\zeta_{i,j-1}^{n}]}{2\Delta Y}$$
$$=Pr\left\{\frac{[\zeta_{i+1,j}^{n+1}-2\zeta_{i,j}^{n+1}+\zeta_{i-1,j}^{n+1}]}{\Delta X^2}+\frac{[\zeta_{i,j+1}^{n}-2\zeta_{i,j}^{n+1}+\zeta_{i,j-1}^{n}]}{\Delta Y^2}\right\}$$
$$+Ra_{\mathrm{T}}Pr\left\{-\frac{[\theta_{i+1,j}-\theta_{i-1,j}]}{2\Delta X}+N\frac{[C_{i+1,j}-C_{i-1,j}]}{2\Delta X}\right\}$$
$$-Ha^2Pr\frac{[V_{i+1,j}-V_{i-1,j}]}{2\Delta X}, \tag{15a}$$

which can be rearranged as

$$\zeta_{i-1,j}^{n+1}[E_1]+\zeta_{i,j}^{n+1}[B_1]+\zeta_{i+1,j}^{n+1}[A_1]=[D_1], \tag{15b}$$

where

$$E_1=\left[-\frac{U_{i,j}\Delta\tau}{2\Delta X}-\frac{Pr\,\Delta\tau}{\Delta X^2}\right],\quad B_1=\left[1.0+\frac{2Pr\,\Delta\tau}{\Delta X^2}+\frac{2Pr\,\Delta\tau}{\Delta Y^2}\right]$$
$$A_1=\left[-\frac{U_{i,j}\Delta\tau}{2\Delta X}-\frac{Pr\,\Delta\tau}{\Delta X^2}\right],$$
$$D_1=\zeta_{i,j+1}^{n}\left[-\frac{V_{i,j}\Delta\tau}{2\Delta Y}-\frac{Pr\,\Delta\tau}{\Delta Y^2}\right]+\zeta_{i,j}^{n}[1.0]$$
$$+\zeta_{i,j-1}^{n}\left[\frac{V_{i,j}\Delta\tau}{2\Delta Y}+\frac{Pr\,\Delta\tau}{\Delta Y^2}\right]$$
$$+Ra_{\mathrm{T}}Pr\,\Delta\tau\left\{-\frac{[\theta_{i+1,j}-\theta_{i-1,j}]}{2\Delta X}+N\frac{[C_{i+1,j}-C_{i-1,j}]}{2\Delta X}\right\}$$
$$-Ha^2Pr\,\Delta\tau\frac{[V_{i+1,j}-V_{i-1,j}]}{2\Delta X}. \tag{15c}$$

The finite-difference formulation for Eq. (11) will be written as

$$\frac{\left[\theta_{i,j}^{n+1}-\theta_{i,j}^{n}\right]}{\Delta\tau}+U_{i,j}\frac{\left[\theta_{i+1,j}^{n+1}-\theta_{i-1,j}^{n+1}\right]}{2\Delta X}+V_{i,j}\frac{\left[\theta_{i,j+1}^{n}-\theta_{i,j-1}^{n}\right]}{2\Delta Y}$$
$$=\left\{\frac{\left[\theta_{i+1,j}^{n+1}-2\theta_{i,j}^{n+1}+\theta_{i-1,j}^{n+1}\right]}{\Delta X^2}+\frac{\left[\theta_{i,j+1}^{n}-2\theta_{i,j}^{n}+\theta_{i,j-1}^{n}\right]}{\Delta Y^2}\right\}$$
$$+\phi\left[\theta_{i,j}^{n+1}+0.5\right], \tag{16a}$$

which can be rearranged as

$$\theta_{i-1,j}^{n+1}[E_1]+\theta_{i,j}^{n+1}[B_1]+\theta_{i+1,j}^{n+1}[A_1]=[D_1], \tag{16b}$$

where

$$E_1=\left[-\frac{U_{i,j}\Delta\tau}{2\Delta X}-\frac{\Delta\tau}{\Delta X^2}\right],\quad B_1=\left[1.0+\frac{2\Delta\tau}{\Delta X^2}-\phi\Delta\tau\right],$$
$$A_1=\left[-\frac{U_{i,j}\Delta\tau}{2\Delta X}-\frac{\Delta\tau}{\Delta X^2}\right],$$
$$D_1=\theta_{i,j+1}^{n}\left[-\frac{V_{i,j}\Delta\tau}{2\Delta Y}+\frac{\Delta\tau}{\Delta Y^2}\right]+\theta_{i,j}^{n}\left[1.0-\frac{2\Delta\tau}{\Delta Y^2}\right]$$
$$+\theta_{i,j-1}^{n}\left[\frac{V_{i,j}\Delta\tau}{2\Delta Y}+\frac{\Delta\tau}{\Delta Y^2}\right]+\frac{\phi\Delta\tau}{2}. \tag{16c}$$

The finite-difference formulation for Eq. (12) can be written as

$$\frac{\left[C_{i,j}^{n+1}-C_{i,j}^{n}\right]}{\Delta\tau}+U_{i,j}\frac{\left[C_{i+1,j}^{n+1}-C_{i-1,j}^{n+1}\right]}{2\Delta X}+V_{i,j}\frac{\left[C_{i,j+1}^{n}-C_{i,j-1}^{n}\right]}{2\Delta Y}$$
$$=\frac{1}{Le}\left\{\frac{\left[C_{i+1,j}^{n+1}-2C_{i,j}^{n+1}+C_{i-1,j}^{n+1}\right]}{\Delta X^2}+\frac{\left[C_{i,j+1}^{n}-2C_{i,j}^{n}+C_{i,j-1}^{n}\right]}{\Delta Y^2}\right\}, \tag{17a}$$

which can be rearranged as

$$C_{i-1,j}^{n+1}[E_1]+C_{i,j}^{n+1}[B_1]+C_{i+1,j}^{n+1}[A_1]=[D_1], \tag{17b}$$

where

$$E_1=\left[-\frac{U_{i,j}\Delta\tau}{2\Delta X}-\frac{\Delta\tau}{Le\,\Delta X^2}\right],\quad B_1=\left[1.0+\frac{2\Delta\tau}{Le\,\Delta X^2}\right],$$
$$A_1=\left[-\frac{U_{i,j}\Delta\tau}{2\Delta X}-\frac{\Delta\tau}{Le\,\Delta X^2}\right]$$
$$D_1=C_{i,j+1}^{n}\left[-\frac{V_{i,j}\Delta\tau}{2\Delta Y}+\frac{\Delta\tau}{Le\,\Delta Y^2}\right]+C_{i,j}^{n}\left[1.0-\frac{2\Delta\tau}{Le\,\Delta Y^2}\right]$$
$$+C_{i,j-1}^{n}\left[\frac{V_{i,j}\Delta\tau}{2\Delta Y}+\frac{\Delta\tau}{Le\,\Delta Y^2}\right], \tag{17c}$$

U and V can be determined explicitly from

$$U_{i,j}^{n+1}=\frac{[\psi_{i,j+1}-\psi_{i,j-1}]}{2\Delta Y},\quad V_{i,j}^{n+1}=\frac{[\psi_{i+1,j}-\psi_{i-1,j}]}{2\Delta X}. \tag{18}$$

The finite-difference formulation for the boundary condition (13b)–(13e) is

$Y=0$ (*horizontal top wall*):

$$\zeta=-\left(\frac{\partial^2\psi}{\partial Y^2}\right)\ \Rightarrow\ \zeta_{i,1}^{n+1}=-\frac{[2\psi_{i,1}^{n}-5\psi_{i,2}^{n}+4\psi_{i,3}^{n}-\psi_{i,4}^{n}]}{\Delta Y^2}, \tag{19}$$

$$\frac{\partial\theta}{\partial Y}=0\ \Rightarrow\ \theta_{i,j}^{n+1}=\frac{[4\theta_{i,2}^{n}-\theta_{i,3}^{n}]}{3.0}, \tag{20}$$

$$\frac{\partial C}{\partial Y}=0\ \Rightarrow\ C_{i,j}^{n+1}=\frac{[4C_{i,2}^{n}-C_{i,3}^{n}]}{3.0}. \tag{21}$$

$Y=H/W$ (*horizontal bottom wall*):

$$\zeta=-\left(\frac{\partial^2\psi}{\partial Y^2}\right)\ \Rightarrow\ \zeta_{i,j\,\max}^{n+1}$$
$$=-\frac{[-\psi_{i,j\,\max-3}^{n}+4\psi_{i,j\,\max-2}^{n}-5\psi_{i,j\,\max-1}^{n}+2\psi_{i,j\,\max}^{n}]}{\Delta Y^2}, \tag{22}$$

$$\frac{\partial\theta}{\partial Y}=0\ \Rightarrow\ \theta_{i,j\,\max}^{n+1}=\frac{[4\theta_{i,j\,\max-1}^{n}-\theta_{i,j\,\max-2}^{n}]}{3.0}, \tag{23}$$

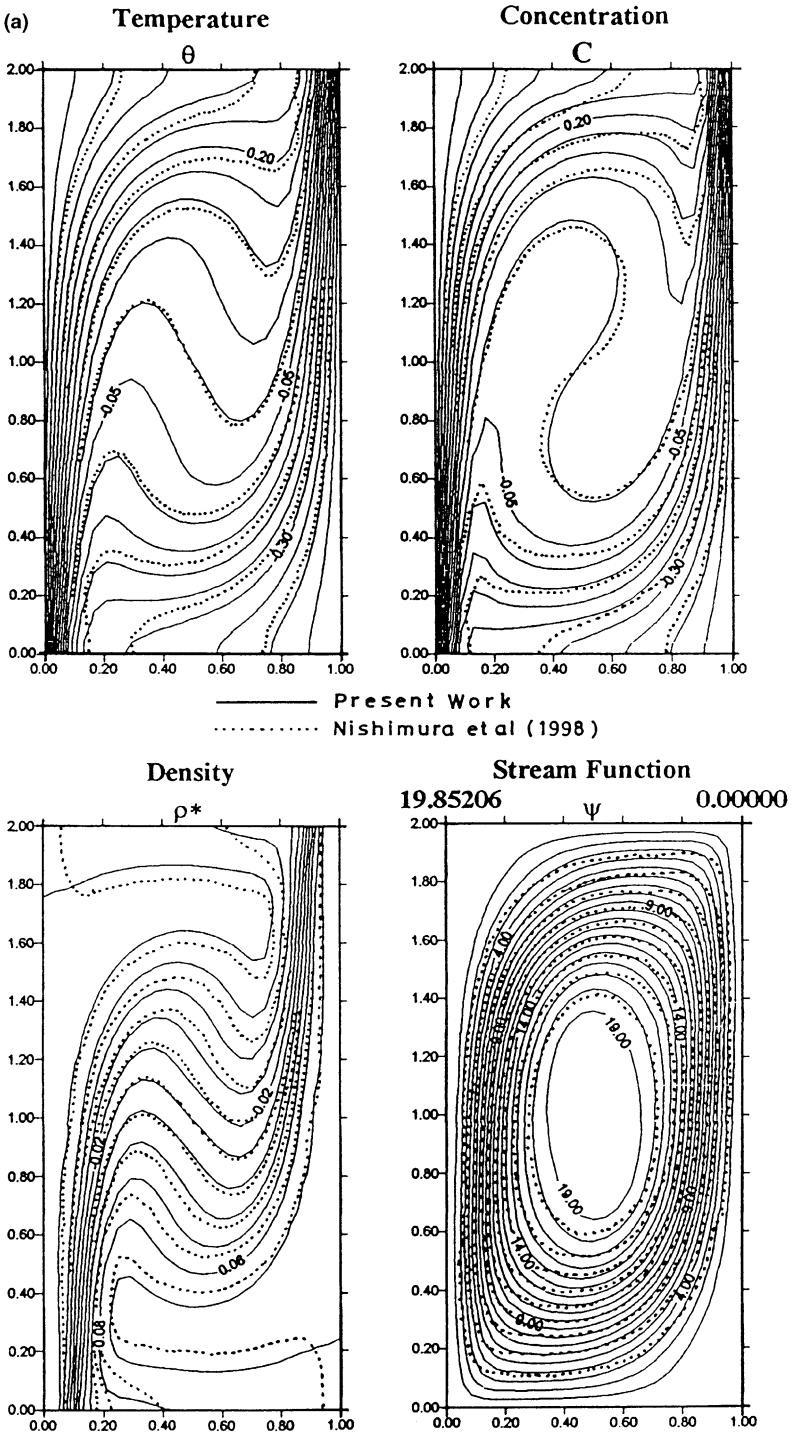

Fig. 2. (a) Steady thermal-dominated solution for $N = 0.8$, $Ha = 0.0$, $\phi = 0.0$. (b) Steady compositional-dominated solution for $N = 1.3$, $Ha = 0.0$, $\phi = 0.0$.

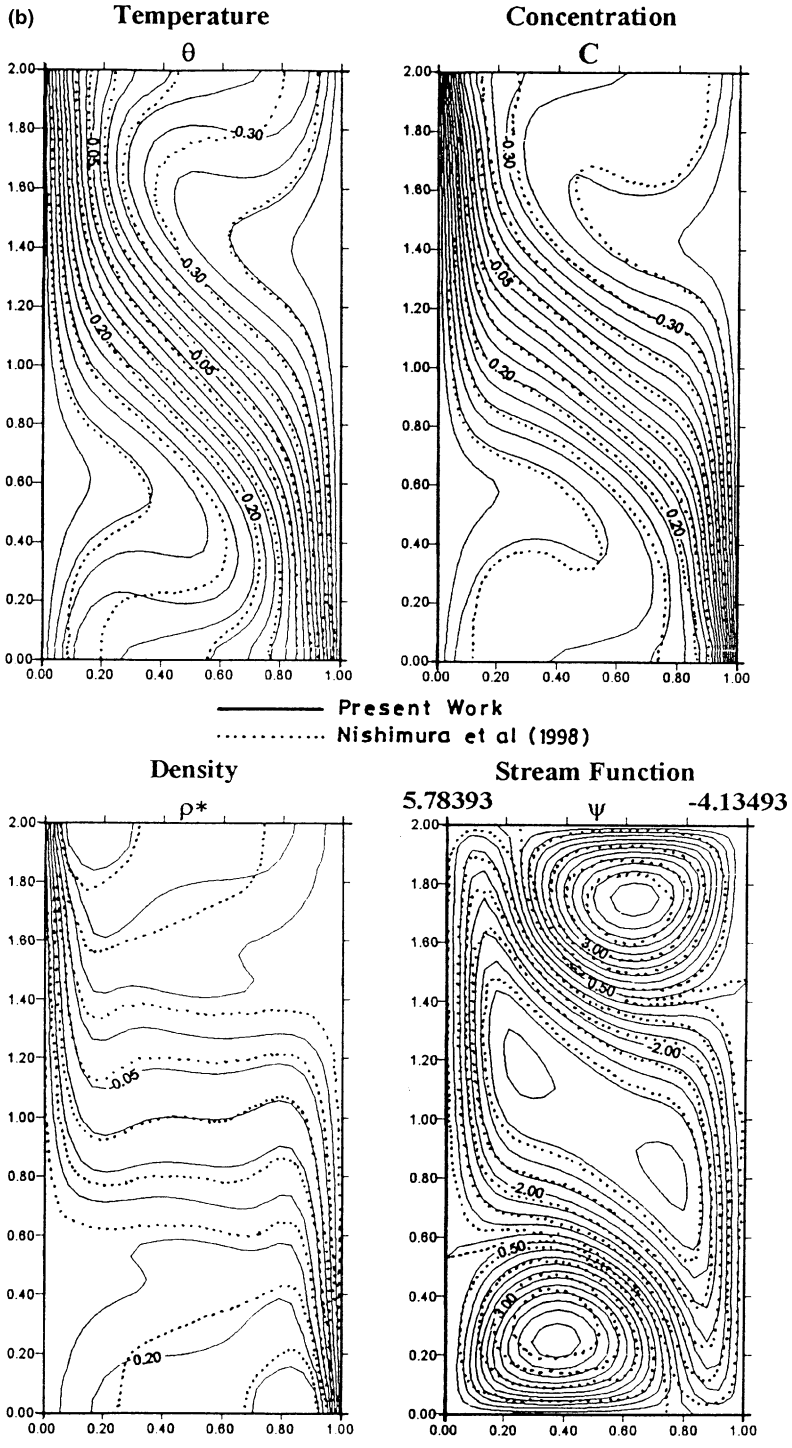

Fig. 2. (*Continued*).

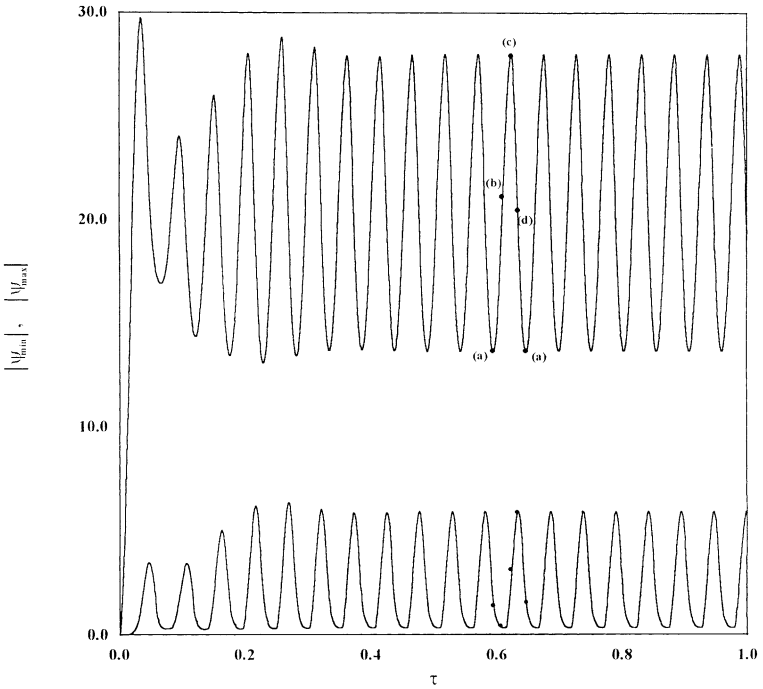

Fig. 3. Oscillatory behavior of $|\psi_{\min}|$ and $|\psi_{\max}|$ with time for $Ha = 0.0$, $Le = 2.0$, $N = 1.0$, $Pr = 1.0$, $Ra_T = 10^5$, and $\phi = 0.0$.

$$\frac{\partial C}{\partial Y} = 0 \;\Rightarrow\; C^{n+1}_{i,j\,\max} = \frac{[4C^{n}_{i,j\,\max-1} - C^{n}_{i,j\,\max-2}]}{3.0}. \tag{24}$$

$X = 0$ (*vertical left wall*):

$$\zeta = -\left(\frac{\partial^2\psi}{\partial X^2}\right) \;\Rightarrow\; \zeta^{n+1}_{1,j} = 2\frac{[\psi^{n}_{1,j} - \psi^{n}_{2,j}]}{\Delta X^2}, \tag{25}$$

$$\theta^{n+1}_{1,j} = 0.5, \quad C^{n+1}_{1,j} = 0.5. \tag{26}$$

$X = 1$ (*vertical right wall*):

$$\zeta = -\left(\frac{\partial^2\psi}{\partial X^2}\right) \;\Rightarrow\; \zeta^{n+1}_{i\,\max,j} = 2\frac{[\psi^{n}_{i\,\max,j} - \psi^{n}_{i\,\max-1,j}]}{\Delta X^2}, \tag{27}$$

$$\theta^{n+1}_{i\,\max,j} = -0.5, \quad C^{n+1}_{i\,\max,j} = -0.5. \tag{28}$$

The subscripts i and j denote the X and Y locations. The superscripts n and $n+1$ denote the time steps, respectively. The computation is carried out for 31×41 grid nodal points for a time step of 10^{-5}, $\Delta X = 1/30$ and $\Delta Y = 1/20$. The convergence criterion required that the difference between the current and previous iterations for all of the dependent variables be 10^{-4}.

The Nusselt and Sherwood numbers are averaged and evaluated along the left boundary of the enclosure which may be expressed as

$$\overline{Nu} = -\int_0^2 \left(\frac{\partial\theta}{\partial X}\right) \mathrm{d}Y, \tag{29}$$

$$\overline{Sh} = -\int_0^2 \left(\frac{\partial C}{\partial X}\right) \mathrm{d}Y. \tag{30}$$

4. Solution procedure

1. All dependent variables are initialized to zero.
2. The new boundary condition values at $(n+1)$ are calculated for all walls from the previous values at (n).
3. The new concentration values at $(n+1)$ are calculated from the previous (n) values, and then a subroutine is called to solve the obtained tridiagonal equations for all the concentration values at all the internal grid points.
4. The temperature, vorticity, and the stream function are calculated in the same way as in step (3), respectively,
5. The velocity components U and V are calculated at $(n+1)$ from the values at (n) explicitly for all the internal grid points.
6. The error is calculated for the concentration, temperature, and vorticity at the last time step (only for steady solution).
7. The same procedure is followed by starting with step (2) to obtain the solution at the next time step at $(n+2)$.

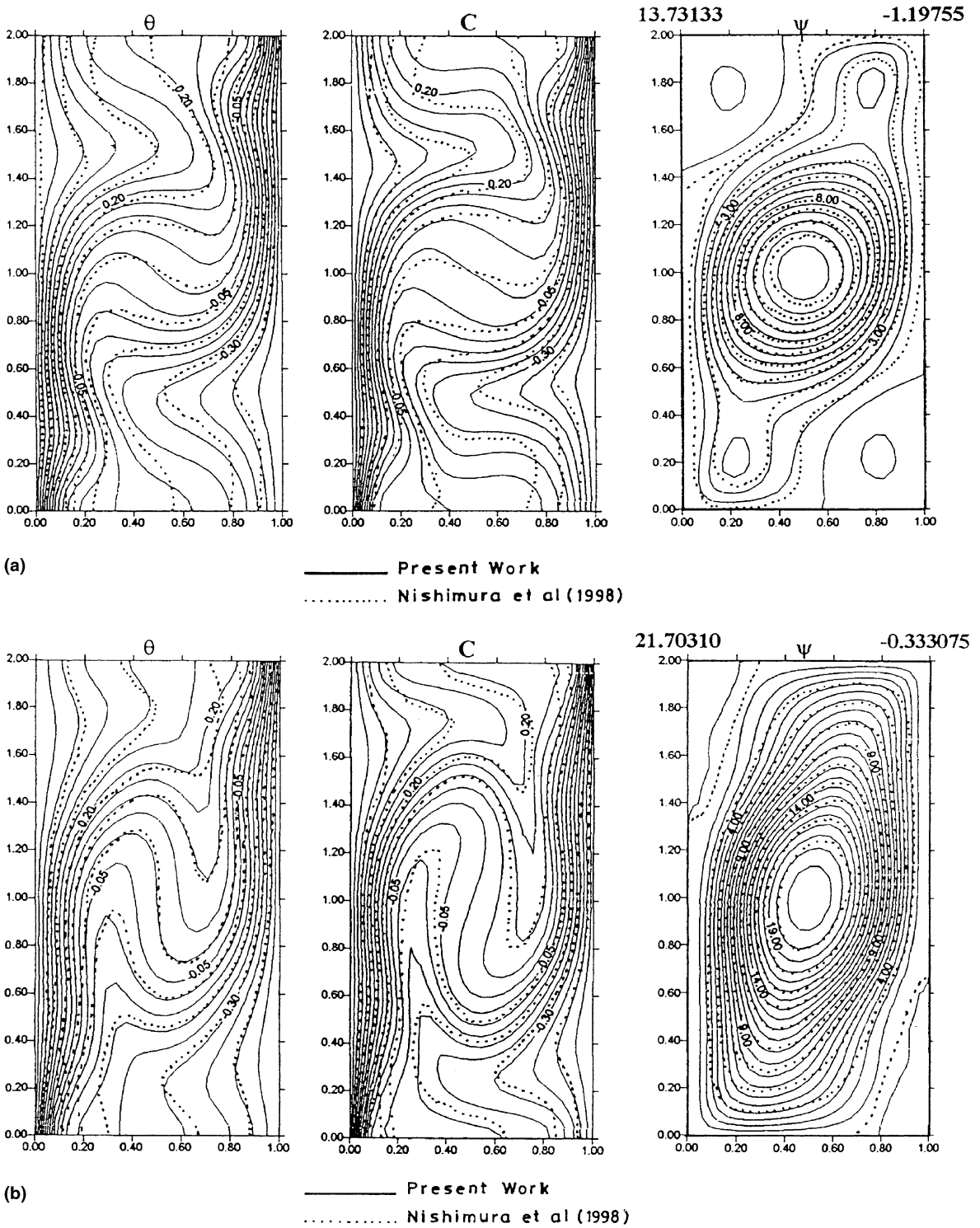

Fig. 4. Case (a) Temperature, concentration, density and streamline contours during a period of oscillation for $N = 1.0$, $Ha = 0.0$, $\phi = 0.0$. Case (b) Temperature, concentration, density and streamline contours during a period of oscillation for $N = 1.0$, $Ha = 0.0$, $\phi = 0.0$. Case (c) Temperature, concentration, density and streamline contours during a period of oscillation for $N = 1.0$, $Ha = 0.0$, $\phi = 0.0$. Case (d) Temperature, concentration, density and streamline contours during a period of oscillation for $N = 1.0$, $Ha = 0.0$, $\phi = 0.0$.

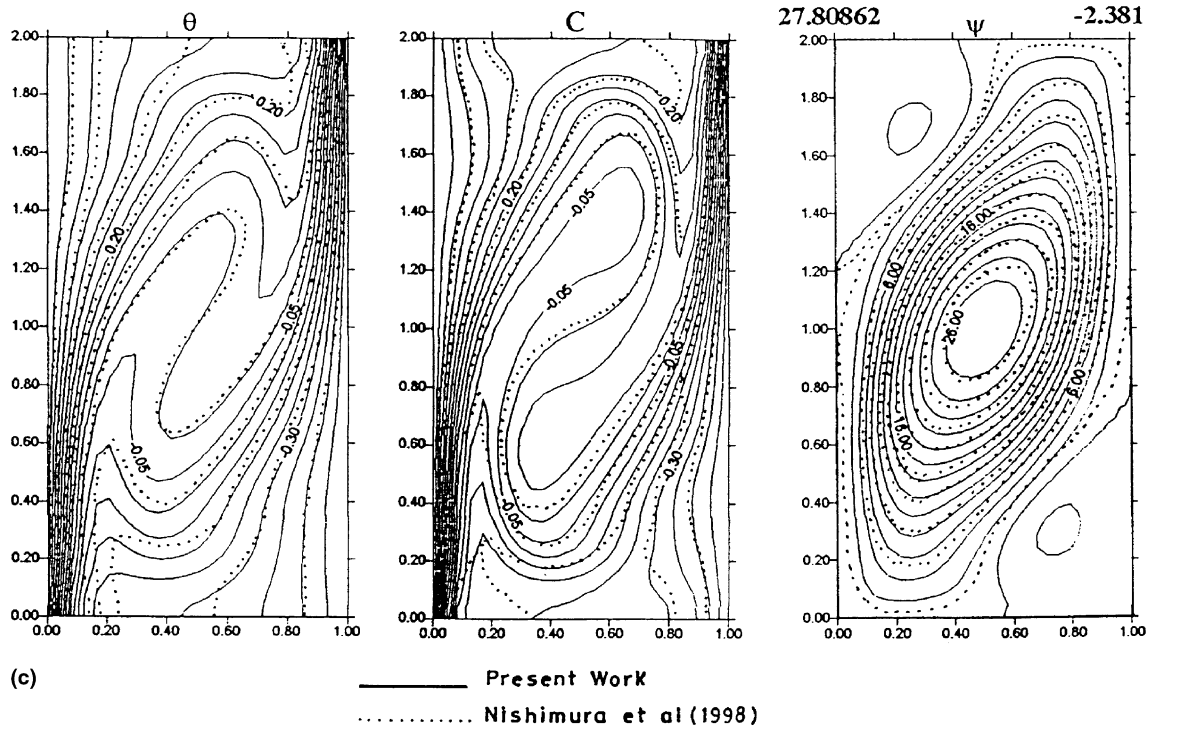

Fig. 4. (*Continued*).

This procedure is for unsteady solution. If the steady solution is required, then the concentration and temperature are only needed to be updated for a number of internal loops for each single time step. Then, at the end of this single time step, the vorticity, stream function, and velocity components (U and V) need to be updated.

8. The average Nusselt and Sherwood numbers are then calculated at the left vertical wall.

5. Numerical validation tests

In order to check on the accuracy of the numerical technique employed for the solution of the problem considered in the present study, it was validated by performing simulation for double-diffusive convection flow in a vertical rectangular enclosure with combined horizontal temperature and concentration gradients and in the absence of the magnetic field and heat generation or absorption effects which was reported earlier by Nishimura et al. [17]. Figs. 2(a) and (b) present comparisons for the streamlines, isotherms, concentration contours and density contours of the present work at $N = 0.8$ (thermal-dominated flow) and $N = 1.3$ (compositional-dominated flow) with those of Nishimura et al. [17]. These comparisons show a good agreement between the results. Fig. 3 illustrates the oscillatory behavior in $|\Psi_{\max}|$ and $|\Psi_{\min}|$ with time predicted by zNishimura et al. [17]. As predicted by these authors, the period of oscillation τ_0 was found to be 0.05091. Also, Figs. 4(a)–(d) corresponding to points a, b, c and d in Fig. 3, respectively, predict the oscillatory behavior with time in the thermal and compositional recirculations at $N = 1.0$ through the streamline, temperature, concentration, and density contours which compare well with the results reported by Nishimura et al. [17]. Moreover, Table 1 shows a favorable comparison between numerical results for a period of oscillation and stream function extrema $|\psi_{\max}|$ and $|\psi_{\min}|$ at $N = 1.0$ obtained by three different numerical schemes: the finite-element method, spectral method (reported by Nishimura et al. [17]) and the finite-difference method of the present work. These various comparisons lend confidence in the numerical results to be reported subsequently.

6. Result and discussion

In this section, numerical results for the streamline, temperature, concentration and density contours as well as selected velocity, temperature and concentration profiles at mid-section of the enclosure for various values of Hartmann number Ha and the heat generation or absorption coefficient ϕ will be reported. In addition, representative results for the average Nusselt number $\overline{Nu}$ and the average Sherwood number $\overline{Sh}$ at various conditions will be presented and discussed.

Fig. 5 presents steady-state contours for the streamline, temperature, concentration, and density at various values of the Hartmann number Ha for $Le = 2.0$, $N = 0.8$, $Pr = 1.0$, $Ra_T = 10^5$ and $\phi = 0.0$. As mentioned by Nishimura et al. [17], when $N < 1.0$ the flow is primarily dominated by thermal buoyancy effects while for $N > 1.0$ the flow is mainly dominated by compositional buoyancy effects. The interaction between the thermal and compositional buoyancy effects is small except for values of N close to unity where these buoyancy effects are of the same order of magnitude but in opposite directions. Therefore, for $N = 0.8$, thermal buoyancy dominates and a large central clockwise thermal recirculation is predicted with the isotherms not being horizontally uniform in the core region within the enclosure. Furthermore, the concentration contours are distorted in the core of the enclosure while the density contours indicate a stable stratification in the vertical direction except near the insulated walls of the enclosure. A stagnant zone in the corners of the enclosure is also observed. The application of the magnetic field is observed to cause the streamlines to be distorted with the formation of a smaller thermal and slower clockwise recirculation in the core region. For large values of Ha the recirculation cell is stretched covering the stagnant zone in the corners and then splits into two smaller thermal circulating cells situated close to each of the insulated upper and bottom walls. The temperature and concentration contours tend to become more similar except in the core region as the Ha increases causing the density contours to become more horizontally uniform for $Ha = 10$ and stably stratified in the core region away front the walls of the enclosure. Also, for very large Hartmann numbers ($Ha = 50$) the isotherms and

Table 1
Comparison between the present method and two numerical methods for $N = 1.0$

	Finite-element method (31×41 points) [17]	Spectral method (40×80 points) [15]	Finite-difference method (31×41 points) present results
τ_0	0.0497	0.0494	0.05091
Max $\lvert\psi_{\max}\rvert$	26.7	26.8	27.8
Min $\lvert\psi_{\max}\rvert$	12.9	12.7	13.7
Max $\lvert\psi_{\min}\rvert$	5.76	5.52	5.85
Min $\lvert\psi_{\max}\rvert$	0.351	0.333	0.333

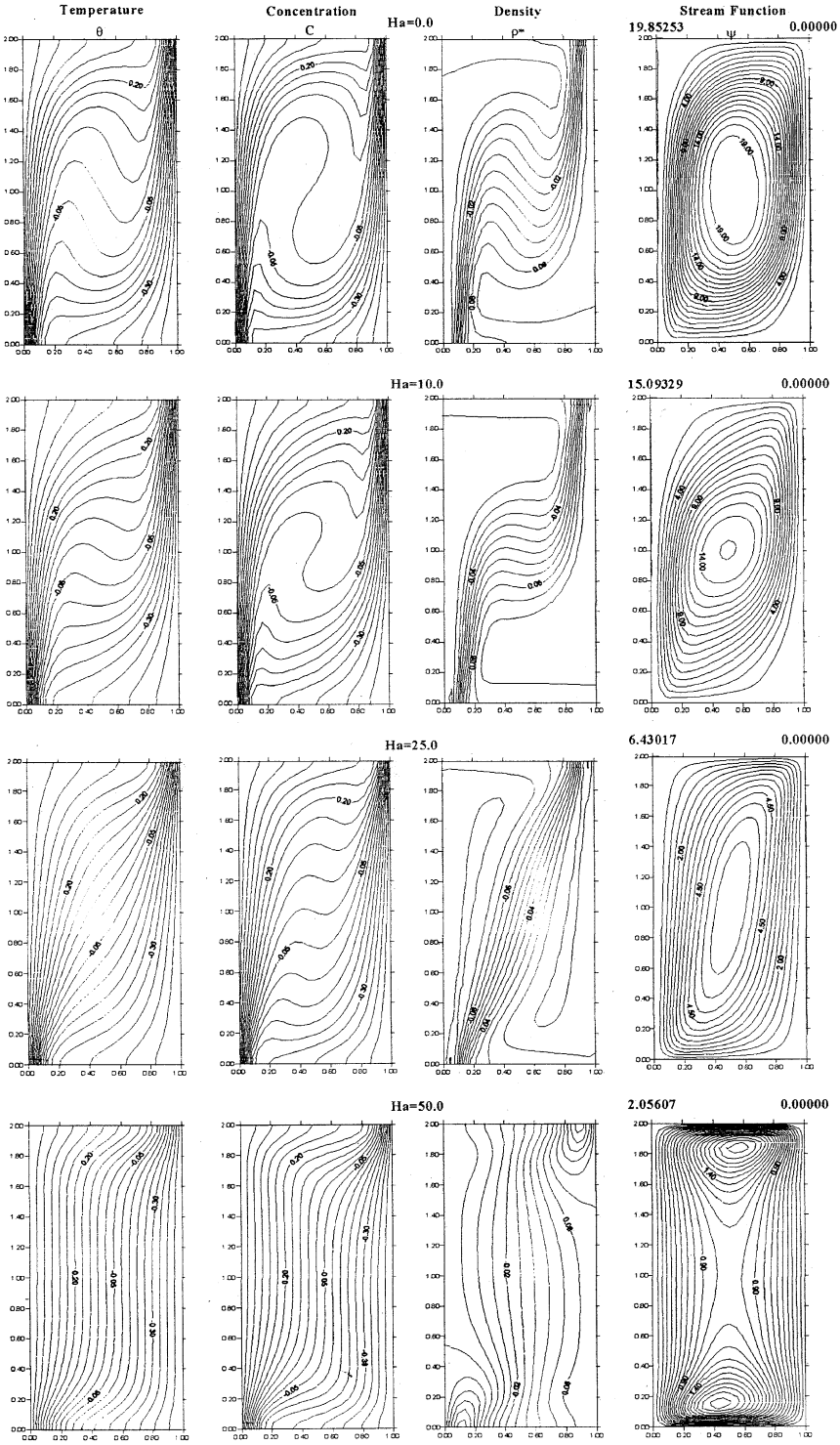

Fig. 5. Steady thermal-dominated solution for $Le = 2.0$, $N = 0.8$, $Pr = 1.0$, $Ra_T = 10^5$, and $\phi = 0.0$.

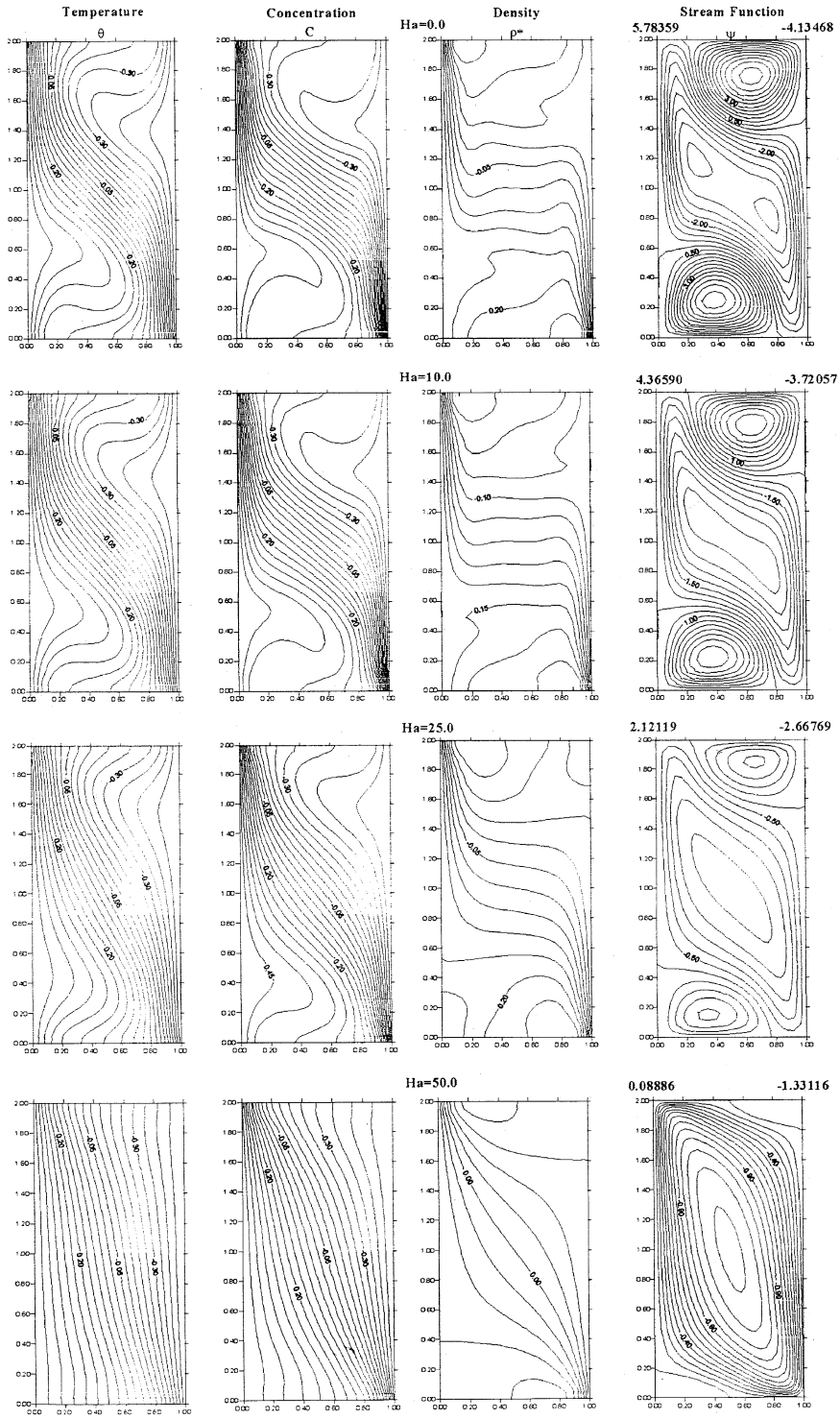

Fig. 6. Steady compositional-dominated solution for $Le = 2.0$, $N = 1.3$, $Pr = 1.0$, $Ra_T = 10^5$, and $\phi = 0.0$.

isoconcentration contours are parallel to the vertical walls except in the immediate vicinity of the horizontal walls indicating the approach to a conduction regime. A main contribution of the application of the magnetic field is seen to suppress the overall heat transfer in the enclosure.

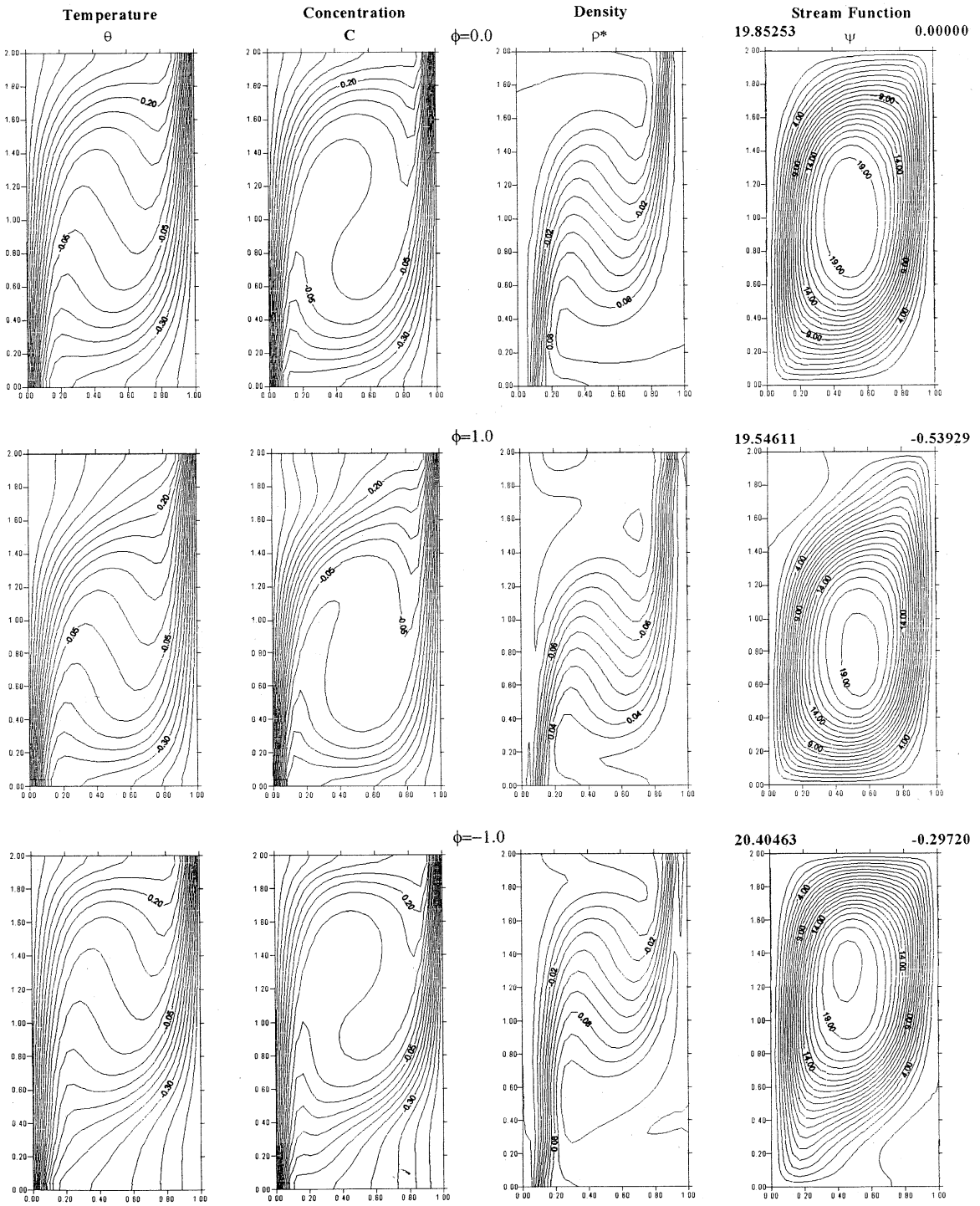

Fig. 7. Steady thermal-dominated solution for $Ha = 0.0$, $Le = 2.0$, $N = 0.8$, $Pr = 1.0$, and $Ra_T = 10^5$.

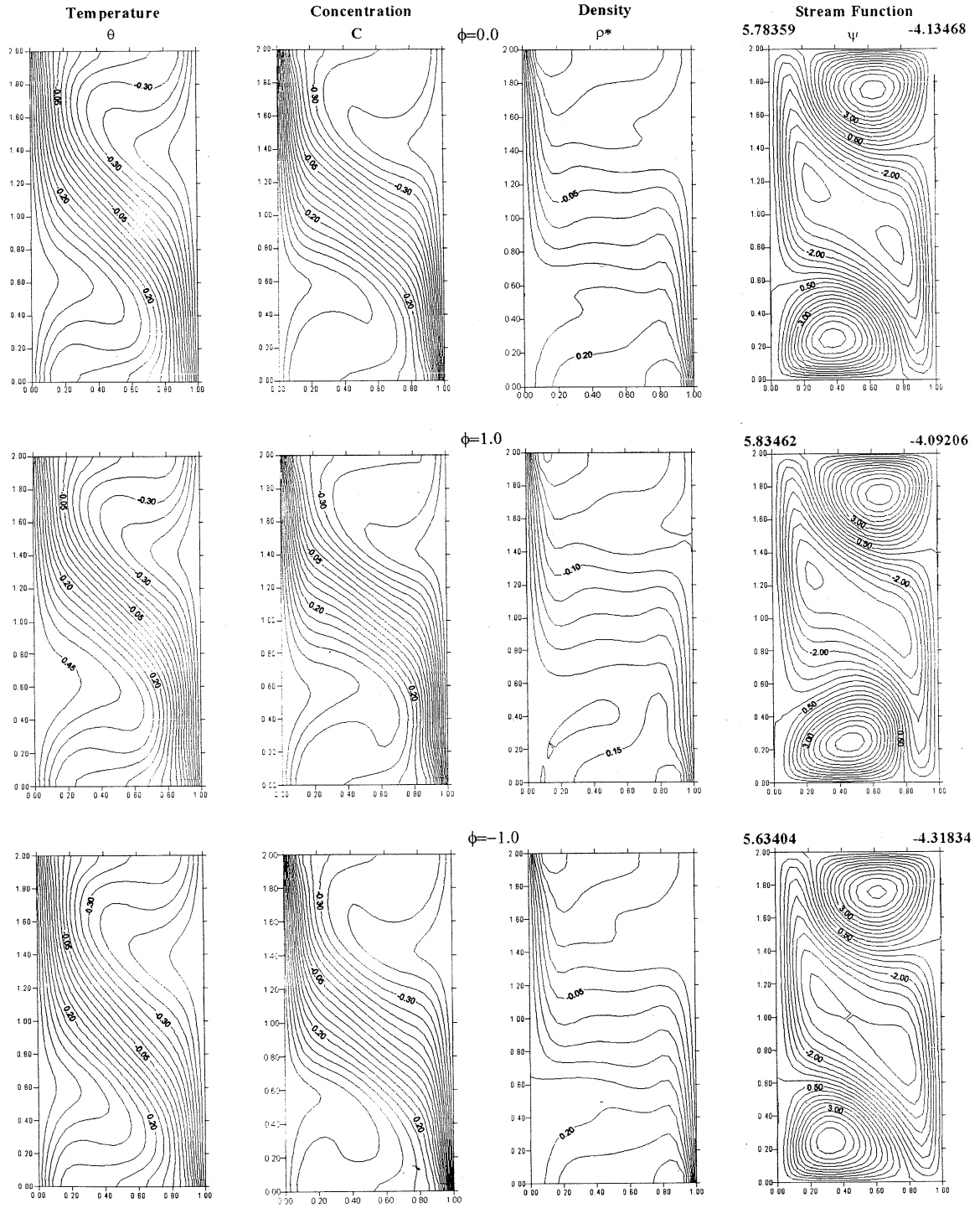

Fig. 8. Steady compositional-dominated solution for $Ha = 0.0$, $Le = 2.0$, $N = 1.3$, $Pr = 1.0$, and $Ra_T = 10^5$.

Fig. 6 displays similar results as shown in Fig. 5 except for $N = 1.3$. For this specific value of N, the flow is dominated by compositional buoyancy effects. In this case, a counterclockwise compositional recirculation exists in the core region of the enclosure along with two clockwise thermal recirculations occurring near the top right and bottom left corners of the enclosure. The contours for temperature and concentration are almost parallel to each other within the center of the enclosure away from the walls that produces more horizontally uniform density contours that are stably stratified in the vertical direction. Similar trends in the flow patterns are predicted where the two clockwise thermal recirculations become smaller and the counterclockwise compositional recirculation is slowed down as Ha increases. For large values of Ha ($Ha = 50$) the two thermal recirculations are eliminated and the flow within the enclosure is circulating at a slower rate due to compositional buoyancy effects. The other contours appear to change slightly as Ha increases.

In Fig. 7, it is observed, for $N = 0.8$, that the presence of a heat sink (heat absorption, $\phi < 0$) within the enclosure causes higher heat transfer rates with the thermal recirculation within the enclosure moving upward with a slightly faster clockwise circulation. However, the presence of a heat source (heat generation, $\phi > 0$) produces less heat transfer rates and the thermal recirculation tends to move downward with a slightly slower clockwise circulation. The stream functions in Fig. 8 show a totally opposite behavior than that predicted in Fig. 7. For $N = 1.3$, heat absorption is seen to slow down the circulations in the enclosure while heat generation speeds them up.

The effects of the Hartmann number Ha and the heat generation or absorption coefficient ϕ on the average Nusselt number $\overline{Nu}$ and the average Sherwood number $\overline{Sh}$ for a buoyancy ratio of $N = 0.8$ are presented in Figs. 9 and 10, respectively. It is observed that both $\overline{Nu}$ and $\overline{Sh}$ have a decreasing trend with increases in Ha. In addition, it is observed that heat generation ($\phi > 0$) decreases the average Nusselt number while heat absorption ($\phi < 0$) increases it. However, both heat generation ($\phi > 0$) and heat absorption ($\phi < 0$) decrease the average Sherwood number. As expected, the effect of the heat generation/absorption coefficient ϕ is more pronounced on the values of $\overline{Nu}$ than on $\overline{Sh}$.

A similar set of results for $\overline{Nu}$ and $\overline{Sh}$ as those reported in Figs. 9 and 10 is illustrated in Figs. 11 and 12 for $N = 1.3$. It is interesting to observe a different behavior for $\overline{Sh}$ in these figures as compared with those corresponding to $N = 0.8$. In these figures, both $\overline{Nu}$ and $\overline{Sh}$ increase as the heat absorption effect increases while they decrease as Ha or ϕ increases. This is associated with the fact that for this case the flow is dominated by compositional buoyancy effects.

Figs. 13 and 14 illustrate the influence of the buoyancy ratio N on the average Nusselt and Sherwood numbers $\overline{Nu}$ and $\overline{Sh}$ for three different Hartmann number values, respectively. It is interesting to observe from these figures the existence of minimum values in $\overline{Nu}$ and $\overline{Sh}$ for a critical buoyancy ratio N_{cr} of about 1.2. The values of $\overline{Nu}$ and $\overline{Sh}$ tend to decrease with increasing values of N for $N < N_{cr}$ and to increase with increasing values of N for $N > N_{cr}$. The existence of such minimum values in $\overline{Nu}$ and $\overline{Sh}$ for a critical value of N has been reported in the literature (see, for instance,

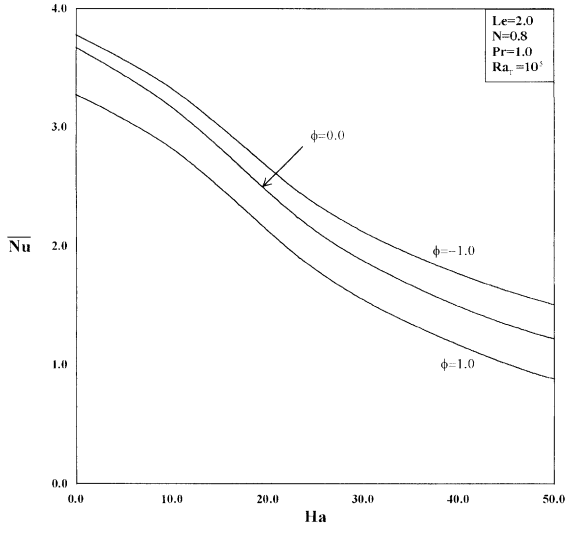

Fig. 9. Average Nusselt number vs. Hartmann number for heat generation/absorption effects.

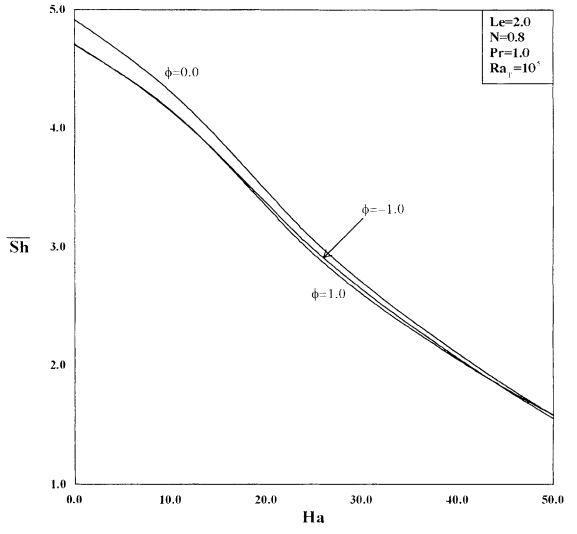

Fig. 10. Average Sherwood number vs. Hartmann number for heat generation/absorption effects.

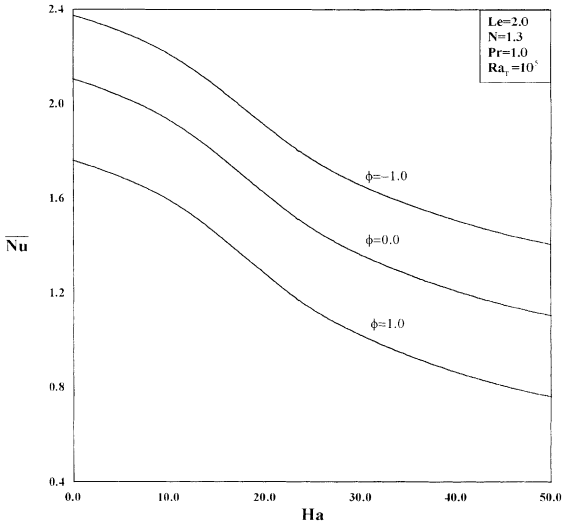

Fig. 11. Average Nusselt number vs. Hartmann number for heat generation/absorption effects.

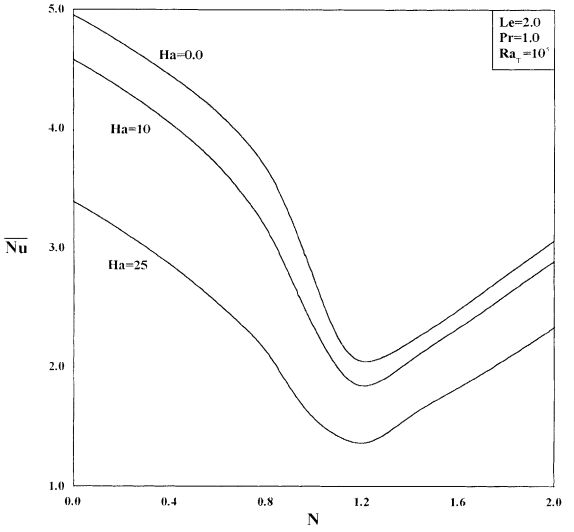

Fig. 13. Average Nusselt number vs. buoyancy ratio for different Hartmann numbers.

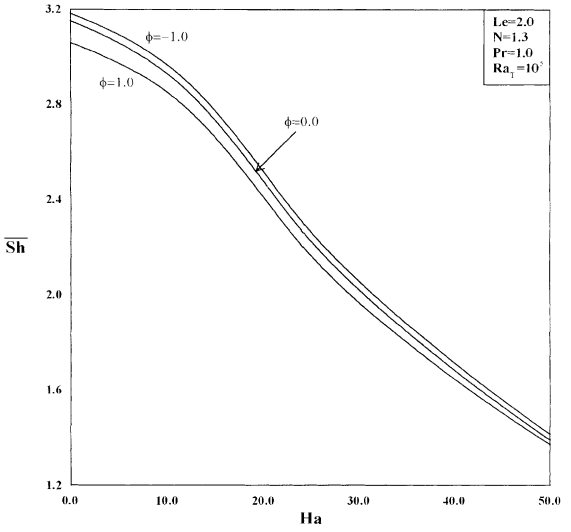

Fig. 12. Average Sherwood number vs. Hartmann number for heat generation/absorption effects.

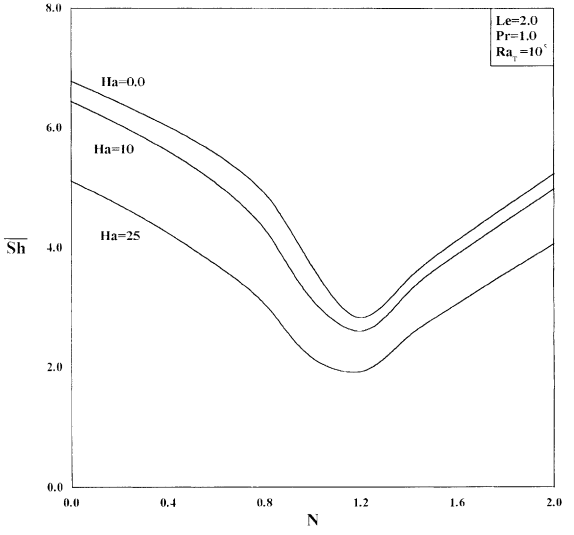

Fig. 14. Average Sherwood number vs. buoyancy ratio for different Hartmann numbers.

[6,16,24]). These behaviors are associated with the thermal-dominated and compositional-dominated regimes discussed earlier.

Finally, Figs. 15 and 16 present the effects of the presence of the magnetic field and heat generation on the transient oscillatory behavior of $|\psi_{\max}|$ and $|\psi_{\min}|$ mentioned before for $N = 1.0$ in comparison with Fig. 3, respectively. It is observed that the presence of a magnetic field in the X-direction decays the oscillatory behavior in $|\psi_{\max}|$ and $|\psi_{\min}|$ as time progresses. This is very important especially in regard to solidification processes such as casting and semiconductor single-crystal growth applications. In these applications, as the liquids undergo solidification, fluid flow and turbulence occur in the solidifying liquid pool and have critical implications on the product quality control. The use of magnetic fields has successfully been applied to controlling melt convection in solidification systems. In Fig. 16, it is clearly seen that the presence of a heat source within the enclosure in the presence of a magnetic

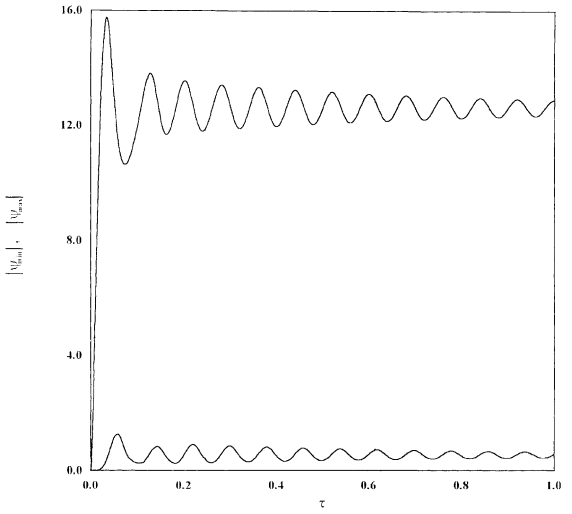

Fig. 15. Oscillatory behavior of $|\psi_{min}|$ and $|\psi_{max}|$ with time for $Ha = 10,\ Le = 2.0,\ N = 1.0,\ Pr = 1.0,\ Ra_T = 10^5$, and $\phi = 0.0$.

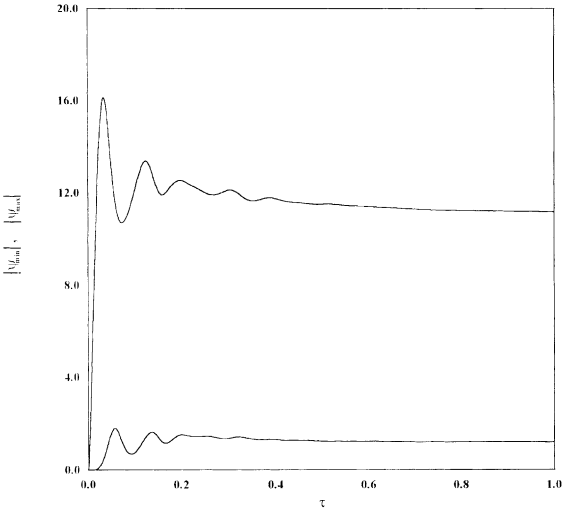

Fig. 16. Oscillatory behavior of $|\psi_{min}|$ and $|\psi_{max}|$ with time for $Ha = 10,\ Le = 2.0,\ N = 1.0,\ Pr = 1.0,\ Ra_T = 10^5$, and $\phi = 1.0$.

field is predicted to speed up the decay of the oscillations in $|\psi_{max}|$ and $|\psi_{min}|$.

7. Conclusions

Unsteady heat and mass transfer by natural convection flow of a heat-generating fluid inside a rectangular enclosure filled with an electrically conducting fluid in the presence of a transverse magnetic field was studied numerically. The finite-difference method was employed for the solution of the present problem. Comparisons with previously published work on special cases of the problem were performed and found to be in good agreement. Graphical results for various parametric conditions were presented and discussed. It was found that the heat and mass transfer mechanisms and the flow characteristics inside the enclosure depended strongly on the strength of the magnetic field and heat generation or absorption effects. The effect of the magnetic field was found to reduce the heat transfer and fluid circulation within the enclosure. In addition, it was concluded that the average Nusselt number was increased owing to the presence of a heat sink while it was decreased when a heat source was present. Furthermore, the periodic oscillatory behavior in the stream function inherent in the problem was decayed by the presence of the magnetic field. This decay in the transient oscillatory behavior was speeded up by the presence of a heat source.

References

[1] S. Acharya, R.J. Goldstein, Natural convection in an externally heated vertical or inclined square box containing internal energy sources, ASME J. Heat Transfer 107 (1985) 855–866.

[2] S. Alchaar, P. Vasseur, E. Bilgen, Natural convection heat transfer in a rectangular enclosure with a transverse magnetic field, ASME J. Heat Transfer 117 (1995) 668–673.

[3] N.M. Al-Najem, K.M. Khanafer, M.M. El-Refaee, Numerical study of laminar natural convection in tilted enclosure with transverse magnetic field, Int. J. Numer. Meth. Heat Fluid Flow 8 (1998) 651–672.

[4] C. Beghein, F. Haghighat, F. Allard, Numerical study of double-diffusive natural convection in a square cavity, Int. J. Heat Mass Transfer 35 (1992) 833–846.

[5] A. Bejan, Mass and heat transfer by natural convection in a vertical cavity, Int. J. Heat Fluid Flow 6 (1985) 149–159.

[6] P. Bera, V. Eswaran, P. Singh, Numerical study of heat and mass transfer in an anisotropic porous enclosure due to constant heating and cooling, Numer. Heat Transfer A 34 (1998) 887–905.

[7] A.J. Chamkha, Non-Darcy fully developed mixed convection in a porous medium channel with heat generation/absorption and hydromagnetic effects, Numer. Heat Transfer 32 (1997) 653–675.

[8] A.G. Churbanov, P.N. Vabishchevich, V.V. Chudanov, V.F Strizhov, A numerical study on natural convection of a heat-generating fluid in rectangular enclosures, Int. J. Heat Mass Transfer 37 (1994) 2969–2984.

[9] J.P. Garandet, T. Alboussiere, R. Moreau, Buoyancy driven convection in a rectangular enclosure with a transverse magnetic field, Int. J. Heat Mass Transfer 35 (1992) 741–748.

[10] J.M. Hyun, J.W. Lee, Double-diffusive convection in a rectangle with cooperating horizontal gradients of temperature and concentration gradients, Int. J. Heat Mass Transfer 33 (1990) 1605–1617.

[11] S. Kakac, W. Aung, R. Viskanta, Natural Convection – Fundamentals and Applications, Hemisphere, Washington, DC, 1985.
[12] Y. Kamotani, L.W. Wang, S. Ostrach, H.D. Jiang, Experimental study of natural convection in shallow enclosures with horizontal temperature and concentration gradients, Int. J. Heat Mass Transfer 28 (1985) 165–173.
[13] J. Lee, M.T. Hyun, K.W. Kim, Natural convection in confined fluids with combined horizontal temperature and concentration gradients, Int. J. Heat Mass Transfer 31 (1988) 1969–1977.
[14] J.W. Lee, J.M. Hyun, Double-diffusive convection in a rectangle with opposing horizontal and concentration gradients, Int. J. Heat Mass Transfer 33 (1990) 1619–1632.
[15] A.M. Morega, T. Nishimura, Double-diffusive convection by Chebyshev collocation method, Technol. Rep. Yamaguchi Univ. 5 (1996) 259–276.
[16] P. Nithiarasu, K.N. Seetharamu, T. Sundararajan, Double-diffusive natural convection in an enclosure filled with fluid-saturated porous medium: a generalized non-Darcy approach, Numer. Heat Transfer A 30 (1996) 413–426.
[17] T. Nishimura, M. Wakamatsu, A.M. Morega, Oscillatory double-diffusive convection in a rectangular enclosure with combined horizontal temperature and concentration gradients, Int. J. Heat Mass Transfer 41 (1998) 1601–1611.
[18] G.M. Oreper, J. Szekely, The effect of an externally imposed magnetic field on buoyancy driven flow in a rectangular cavity, J. Cryst. Growth 64 (1983) 505–515.
[19] S. Ostrach, H.D. Jiang, Y. Kamotani, Thermo-solutal convection in shallow enclosures, in: ASME–JSME Thermal Engineering Joint Conference, Hawaii, 1987.
[20] S. Ostrach, Natural convection with combined driving forces, Physico Chem. Hydrodyn. 1 (1980) 233–247.
[21] H. Ozoe, M. Maruo, Magnetic and gravitational natural convection of melted silicon-two dimensional numerical computations for the rate of heat transfer, JSME 30 (1987) 774–784.
[22] P. Ranganathan, R. Viskanta, Natural convection of a binary gas in rectangular cavities, in: ASME–JSME Thermal Engineering Joint Conference, Hawaii, 1987.
[23] N. Rudraiah, R.M. Barron, M. Venkatachalappa, C.K. Subbaraya, Effect of a magnetic field on free convection in a rectangular enclosure, Int. J. Eng. Sci. 33 (1995) 1075–1084.
[24] O.V. Trevisan, A. Bejan, Mass and heat transfer by natural convection in a vertical slot filled with porous medium, Int. J. Heat Mass Transfer 29 (1986) 403–415.
[25] O.V. Trevisan, A. Bejan, Combined heat and mass transfer by natural convection in a vertical enclosure, ASME J. Heat Transfer 19 (1987) 104–112.
[26] K. Vajravelu, J. Nayfeh, Hydromagnetic convection at a cone and a wedge, Int. Commun. Heat Mass Transfer 19 (1992) 701–710.
[27] R. Viskanta, T.L. Bergman, F.P. Incropera, Double-diffusive natural convection, in: S. Kakac, W. Aung, R. Viskanta (Eds.), Natural Convection: Fundamentals and Applications, Hemisphere, Washington, DC, 1985, pp. 1075–1099.